THE JOURNAL OF PHYSICAL CHEMISTRY C
A JOURNAL OF THE AMERICAN CHEMICAL SOCIETY

pubs.acs.org/JPCC Article

Thermal Atomic Layer Etching of Indium Gallium Zinc Oxide (IGZO), In_2O_3, Ga_2O_3, and ZnO Using Sequential Hydrogen Fluoride and Acetylacetone Exposures

Published as part of The Journal of Physical Chemistry C special issue "Joseph S. Francisco Festschrift".

Troy A. Colleran, Aziz I. Abdulagatov, Jonathan L. Partridge, Andrew S. Cavanagh, and Steven M. George*

Cite This: *J. Phys. Chem. C* 2025, 129, 20223−20233 Read Online

ACCESS | Metrics & More | Article Recommendations

Downloaded via UNIV OF COLORADO BOULDER on January 1, 2026 at 19:43:41 (UTC).
See https://pubs.acs.org/sharingguidelines for options on how to legitimately share published articles.

ABSTRACT: Thermal atomic layer etching (ALE) of indium gallium zinc oxide (IGZO), In_2O_3, Ga_2O_3, and ZnO was achieved using sequential hydrogen fluoride (HF) and acetylacetone (Hacac) exposures. The HF exposure fluorinates the metal oxide surface to a metal fluoride layer. The Hacac exposure then undergoes ligand substitution and hydrogen transfer to volatilize the metal fluoride layer. The etching of IGZO films was studied using *in situ* spectroscopic ellipsometry (SE). Repeated exposures of Hacac or sequential exposures of Hacac and O_3 on IGZO films at temperatures up to 250 °C observed no etching. However, fluorination prior to Hacac exposures achieved IGZO etching. Sequential exposures of HF and Hacac produced etch rates of 0.3 Å/cycle at 200 °C. The etch rates increased with temperature up to an etch rate of 0.6 Å/cycle at 250 °C. Similar experiments were performed using hexafluoroacetylacetone (Hhfac) instead of Hacac. Sequential exposures of HF and Hhfac revealed slightly lower etch rates of 0.2 Å/cycle at 230 °C. The etch rates using HF and Hhfac exposures increased with temperature up to an etch rate of 0.5 Å/cycle at 270 °C. *In situ* quadrupole mass spectrometry (QMS) studies were performed to study the volatile products during etching of In_2O_3, Ga_2O_3, and ZnO powders by sequential HF and Hacac exposures at 200 °C. These QMS investigations observed H_2O during HF fluorination of In_2O_3 and Ga_2O_3. $M(acac)_x$ species where M = In or Ga and HF were also monitored as etch products during Hacac exposures on fluorinated In_2O_3 and Ga_2O_3. These etch products were consistent with a ligand substitution and hydrogen transfer mechanism. The time dependence of the $In(acac)_3^+$ and $Ga(acac)_2^+$ ion signals was monitored during Hacac exposures after fluorination of In_2O_3 and Ga_2O_3. The decay of the $M(acac)_x^+$ ion signal intensity versus Hacac exposure was consistent with a self-limiting surface reaction. In contrast, ZnO was spontaneously etched by Hacac. There was a constant $Zn(acac)_2^+$ ion signal during Hacac exposure on ZnO with no previous fluorination of ZnO. However, this spontaneous etching of ZnO by Hacac did not affect the self-limiting behavior of IGZO thermal ALE films using sequential HF and Hacac exposures.

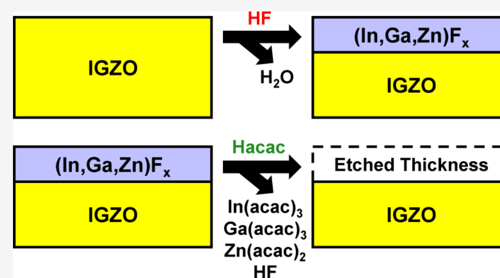

1. INTRODUCTION

Indium gallium zinc oxide (IGZO) is a ternary metal oxide semiconductor that has important applications.[1−3] The transparency and conductivity of IGZO leads to its utilization as a conductor in flat panel displays, solar cells and organic light-emitting diodes.[4] The high electron mobility, reasonable bandgap, and low temperature processing requirements of IGZO facilitate its use as a channel material for thin film transistors.[1−3,5,6] Thin film IGZO is also being developed for flexible electronic devices and sensors.[1,7,8]

The thickness of IGZO films affects the performance of IGZO devices. Thickness is known to define the electrical,[9−13] optical,[14] and gas sensing properties.[15] IGZO thickness can be controlled during film growth using techniques such as atomic layer deposition (ALD).[16−18] The IGZO thickness can also be tuned by etching IGZO films. However, despite the many applications of IGZO in microelectronic devices, transparent conducting layers, and sensors, there are only a limited number of methods available to etch IGZO.

IGZO can be etched using both wet and dry processes. Wet aqueous etching methods for IGZO are based on various acids such as sulfuric, acetic, hydrochloric, and hydrofluoric acid.[19,20] The problem with wet etching is the lack of precision and pattern collapse in small feature sizes resulting from capillary action.[21] Dry etching processes for IGZO have utilized

Received: August 16, 2025
Revised: October 14, 2025
Accepted: October 17, 2025
Published: October 30, 2025

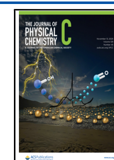

ACS Publications © 2025 American Chemical Society

https://doi.org/10.1021/acs.jpcc.5c05730
J. Phys. Chem. C 2025, 129, 20223−20233

halogen-based plasmas.[22,23] Active ion bombardment via reactive ion etching (RIE) is useful to remove the halide etch products that have low volatility.[24] Switching to hydrocarbon-based plasma can improve IGZO RIE because the organometallic etch products have higher volatility.[25] The problem with plasma methods is the ion-induced surface damage.[26−28]

Thermal atomic layer etching (ALE) methods offer etching precision without ion-induced surface damage. Atomic layer etching (ALE) is a two-step etching process involving sequential, self-limiting surface reactions that provide fine control over the material removal.[29−31] The first step is surface modification of the material. The second step involves volatile release of the modified surface layer.[29−31] ALE can be performed using either thermal or plasma methods.[30,31] In thermal ALE, the volatilization of the modified surface occurs using a thermal reaction.[29,31] Plasma ALE utilizes high energy ions to remove the modified surface layer and can damage the surface.[30]

Several mechanisms for thermal ALE have been developed over the past 10 years.[31] One method is based on fluorination and ligand exchange.[31,32] In this method, fluorination is typically the surface modification reaction, followed by ligand exchange to volatilize the metal.[31,32] This method of thermal ALE has been used to etch many metal oxides, including Al_2O_3,[33−37] and HfO_2.[38−40] Another method of thermal ALE is based on chlorination and ligand addition. Chlorination is the surface modification reaction.[41−43] Ligand addition then volatilizes the metal chloride using precursors such as $P(CH_3)_3$ and tetramethylethylenediamine (TMEDA). Examples of the chlorination and ligand-addition mechanism include Ni and Co ALE.[41,42]

Another chemical pathway for thermal ALE is conversion and volatilization of the converted layer.[31,44] During conversion, the top metal oxide is converted to a different metal oxide that can be volatilized by a second reaction.[31,44−46] Examples of the conversion mechanism include W ALE using sequential O_3, BCl_3 and HF exposures and Al_2O_3 thermal ALE using sequential BCl_3 and HF reactions.[44,46] For both W and Al_2O_3 thermal ALE, BCl_3 converts the metal oxide to a B_2O_3 layer. The B_2O_3 conversion layer is then spontaneously volatilized by fluorination using HF.[45,46] Other examples of conversion mechanisms for thermal ALE include Si, SiO_2, Si_3N_4 and SiGe.[47−50]

Other thermal ALE mechanisms utilize Hacac or Hhfac to form volatile $M(acac)_x$ or $M(hfac)_x$ compounds. Hhfac can spontaneously etch some metal oxides such as ZnO, iron oxide and copper oxide.[51−53] Hacac can also be utilized with O_3 exposures to etch a wide range of first row transition metal oxides such as Cr_2O_3, VO_2 and Sc_2O_3.[54] The O_3 or O_2 plasma exposure can remove carbon residue from the surface or change the oxidation state of the metal oxide.[55,56] The O_3 or O_2 plasma exposure can also oxidize elemental metals prior to Hacac or Hhfac exposures for metal ALE.[57] For these thermal ALE processes, Hacac or Hhfac undergoes ligand substitution and hydrogen transfer with the metal oxide.[56]

Hacac can also react with metal fluorides through a ligand substitution and hydrogen transfer mechanism.[58] This reaction pathway was utilized earlier for the ALE of hafnium zirconium oxide, HfO_2 and ZrO_2 using sequential HF and Hacac exposures.[58] The unusual aspect of these ALE reactions was that HF was a reactant for fluorination and then Hacac produced HF as a reaction product during the volatilization of the metal fluoride.[58] In addition to metal fluorides, Hhfac can also be employed after chlorination of elemental metals, such as Co, to remove the metal chloride.[59,60]

In this paper, sequential exposures of HF and Hacac are employed to etch IGZO, In_2O_3, Ga_2O_3 and ZnO. HF is used for fluorination and Hacac is utilized for ligand substitution and hydrogen transfer with the metal fluoride. The proposed mechanism for IGZO ALE using fluorination and ligand substitution and hydrogen transfer is shown in Figure 1. The ligand substitution and hydrogen transfer reaction is proposed to form volatile $In(acac)_3$, $Ga(acac)_3$, $Zn(acac)_2$, and HF etch products.

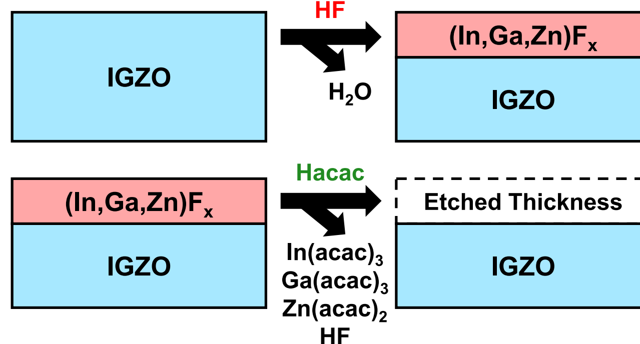

Figure 1. Proposed mechanism for IGZO ALE utilizing HF for fluorination and acetylacetone for ligand substitution and hydrogen transfer.

2. EXPERIMENTAL METHODS

2.1. Grazing Incidence X-ray Diffraction (GI-XRD) and X-ray Reflectivity (XRR). Grazing incidence X-ray diffraction (GI-XRD) was used to characterize the crystallinity of the IGZO films. The density and thickness of the IGZO films were measured by X-ray reflectivity (XRR). The GI-XRD scans were analyzed using Jordan Valley Polycrystal (Jordan Valley Semiconductors). The XRR scans were modeled and fitted using Bede REFS software (Jordan Valley Semiconductors).

Both GI-XRD and XRR scans were accomplished using an X-ray diffractometer (Bede D1, Jordan Valley Semiconductors). These measurements employed radiation from Cu Kα at λ = 1.54 Å. The X-ray tube filament voltage and current were 40 kV and 35 mA, respectively. The incident angle of the X-rays for the GI-XRD scans was 0.3°. The XRR scan range was 300−6000 arcsec with a 5 arcsec step size.

2.2. *In Situ* Spectroscopic Ellipsometry (SE). The IGZO etch experiments were conducted on IGZO thin films provided by Lam Research. GI-XRD analysis revealed that the IGZO thin films were amorphous. XRR investigations also determined that the IGZO films had a thickness of 120 Å and a density of 6.2 g/cm^3. Each IGZO sample was obtained from the same silicon wafer with the deposited IGZO film for consistency. These studies were performed in a warm wall, hot-stage type reactor equipped with a spectroscopic ellipsometer (J.A. Woollam, model M-2000UI). The IGZO film thicknesses were monitored at an incidence angle of 70°.

The IGZO thin film temperature was varied between 200 and 270 °C. The reaction temperatures were controlled by heating of the sample stage using a cartridge heater. The walls of the reactor were maintained at 160 °C. One cycle of IGZO ALE using Hacac consisted of a 0.4 Torr dose of HF for 0.5 s,

followed by a 0.4 Torr dose of Hacac for 0.5 s. Between each dose was a 30 s purge time. *In situ* SE measurements were recorded during each purge time. For comparison, one cycle of IGZO ALE using Hhfac consisted of an HF exposure of 0.4 Torr for 0.5 s. The Hhfac exposure was 0.6 Torr for 0.2 s. A purge time of 30 s separated the HF and Hhfac exposures.

2.3. X-ray Photoelectron Spectroscopy. X-ray photoelectron spectroscopy (XPS) was performed on the IGZO thin film to determine the film composition. The XPS (PHI 5600) was equipped with a monochromatic A1 Kα source at 1486 eV. Spectra were collected using a pass energy of 93.9 eV. The step size was 0.2 eV/step. Depth profiles were obtained using an Ar^+ ion energy of 3.0 keV. The Ar^+ ion beam was rastered over an area ∼4 mm × 4 mm. Data was collected using AugerScan software (RBD Instruments). The resulting XPS data were analyzed using CASA XPS (Casa Software Ltd.) software.

Figure 2 shows the sputter depth-profiling of the IGZO thin film. The IGZO films were sputtered until the IGZO film was completely removed from the underlying silicon wafer. XPS measurements were recorded after 30 s sputtering increments to determine the changes in the IGZO film composition during sputtering. After removing the initial carbon species from the surface by sputtering, the IGZO film contained approximately 15% indium, 10% zinc, 15% gallium, and 60% oxygen. As sputtering proceeded, the removal of the top IGZO film left the underlying silicon substrate. There were no other measurable elements in the IGZO film.

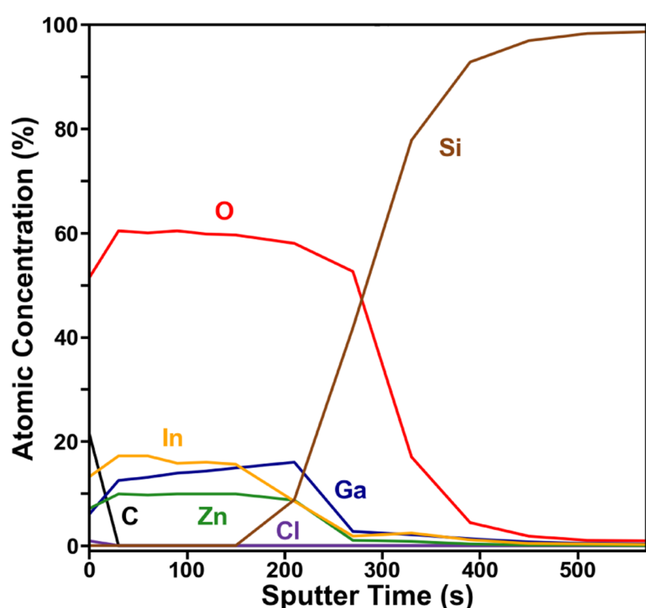

Figure 2. X-ray photoelectron spectroscopy (XPS) sputter depth-profiling of the IGZO thin film.

2.4. Quadrupole Mass Spectrometry (QMS). QMS studies were performed in a chemical reactor that utilizes a dual reactant manifold to provide alternating reactant exposures to high surface area powders.[43] The alternating reactants were flowed through nested inlet lines ending just before the powder bed. This design prevented cross-contamination of the reactant gases. The reactor was also designed to direct the gaseous etch products to a quadrupole mass spectrometer by expansion into vacuum to form a molecular beam.[61] After reacting with the powders, the etch products were transported by a molecular beam expansion.[61] The etch products traveled straight to the ionization region where they were analyzed using a quadrupole mass spectrometer (Extrel MAX-QMS flange-mounted system).[61]

In these QMS experiments, the combined flow rate of the ultrahigh purity N_2 carrier gas through the two reactant manifolds was 2.8 sccm. The N_2 gas flow produced a pressure of ∼2.1 Torr in the sample holder. The N_2 gas was a carrier gas for the reactant and etch products. The N_2 gas was also the purge gas. The HF was derived from a HF-pyridine solution (70% HF, 30% pyridine, Millipore-Sigma). The HF and acetylacetone (≥99% Millipore-Sigma) partial pressures were ∼0.7 Torr. The total pressure during the reactant exposures was ∼2.8 Torr. Experiments were conducted using 120 s exposures of the reactants. These exposures were followed by 300 s purge times to remove the reactant from the powder bed.

The temperature of the powder bed was 200 °C for the QMS experiments. Powders of In_2O_3 (High Purity, 99.995%, US-Nano), Ga_2O_3 (≥99.99% trace metals basis, Sigma), and ZnO (99.9+%, US-Nano), were used in the QMS experiments. These powders were crystalline according to the vendors. Typical powder masses that were loaded into the sample holder were between 40 and 70 mg. The nanopowders varied in diameter from 20 to 200 nm.

For the QMS analysis, the isotopic distributions of the etch products were calculated from the naturally occurring isotopic abundances of each element present in the compound. For example, for $Zn(acac)_2$, where acac is $C_5H_7O_2$, the isotopes of Zn, ^{64}Zn, ^{66}Zn, ^{67}Zn, and ^{68}Zn, and all isotopes of C and O were used to determine the predicted isotopic distribution. The relative abundance was calculated for each m/z value. Some m/z values might contain contributions from more than one distinct chemical species.

3. RESULTS AND DISCUSSION

3.1. IGZO Thermal ALE Using HF and Hacac. Figure 3 shows *in situ* SE results for the change in IGZO film thickness versus number of ALE cycles using sequential HF and Hacac

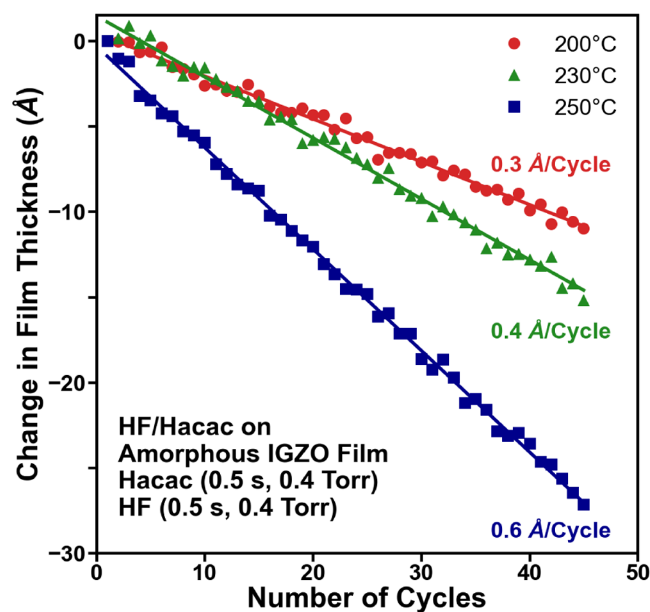

Figure 3. Change in IGZO film thickness measured by *in situ* spectroscopic ellipsometry versus sequential exposures of HF and Hacac at 200 °C, 230 °C, and 250 °C.

https://doi.org/10.1021/acs.jpcc.5c05730
J. Phys. Chem. C 2025, 129, 20223−20233

exposures. The HF exposure was 0.4 Torr for 0.5 s. The Hacac exposure was 0.4 Torr for 0.5 s. A purge time of 30 s separated the HF and Hacac exposures. Temperatures were surveyed from 200 to 250 °C. The change in film thickness was linear with the number of ALE cycles. The measured etch rates were 0.3, 0.4, and 0.6 Å/cycle at 200, 230, and 250 °C, respectively.

Hexafluoroacetylacetone (Hhfac) is another β-diketone closely related to Hacac. Figure 4 shows *in situ* SE results for the change in IGZO film thickness versus number of ALE cycles using sequential HF and Hhfac exposures. The HF exposure was 0.4 Torr for 0.5 s. The Hhfac exposure was 0.6 Torr for 0.2 s. A purge time of 30 s again separated the HF and Hhfac exposures. Temperatures were examined from 230 to 270 °C. The etch rates were smaller for Hhfac compared with Hacac. The measured etch rates were 0.2, 0.4, and 0.5 Å/cycle at 230, 250, and 270 °C, respectively.

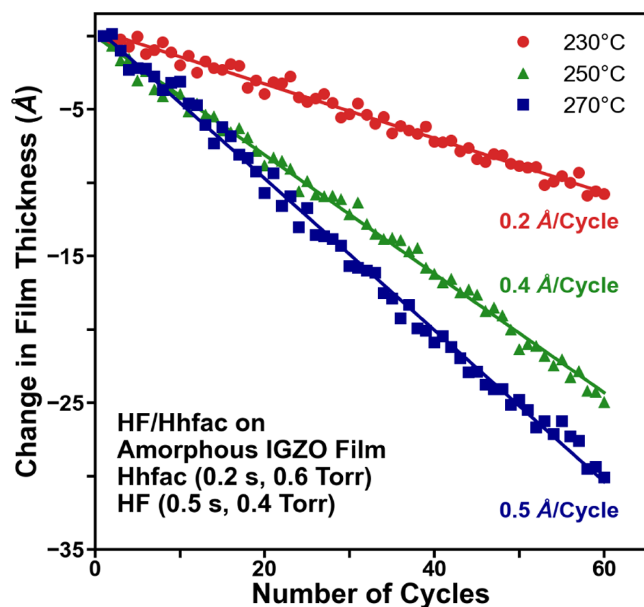

Figure 4. Change in IGZO film thickness measured by *in situ* spectroscopic ellipsometry versus sequential exposures of HF and Hhfac at 230 °C, 250 °C, and 270 °C.

Previous literature suggests that fluorinated β-diketones, such as Hhfac, begin to decompose on ZnO surfaces around 125 °C.[62] In contrast, nonfluorinated β-diketones, such as Hacac, are observed to be stable on ZnO surfaces until around 325 °C.[62] This lower stability for Hhfac may also be observed on ZnF_2 surfaces during ZnO ALE and could lead to the smaller etch rates for ZnO ALE. Because of the smaller etch rates and lower stability with Hhfac, this study concentrated on sequential HF and Hacac exposures for IGZO etching.

Control experiments were also performed to determine the possible etching of IGZO by either Hacac by itself or Hacac together with O_3. The *in situ* SE results showed only a negligible change in IGZO film thickness versus number of cycles using Hacac exposures by themselves or Hacac exposures together with O_3 using either viscous flow or static exposures. The film thickness change was only ~1 Å over 60 cycles. This small thickness change could be attributed to removal of carbon species from the surface or residual fluorine that fluorinates the IGZO surface and leads to a very small etch during the Hacac exposures. These control experiments argued that Hacac by itself or Hacac together with O_3 is not able to etch IGZO.

3.2. In_2O_3 Thermal ALE Using HF and Hacac. QMS studies of etching using HF and Hacac were conducted on the In_2O_3, Ga_2O_3 and ZnO constituent oxides present in IGZO. Figure 5 shows the results for Hacac exposure on fluorinated In_2O_3 powder at 200 °C. The QMS analysis detected a prominent ion intensity at m/z 412. Earlier mass spectrometry studies of $In(acac)_3$ have identified m/z 412 as $In(acac)_3^+$.[63] The largest observed cracking fragment of the $In(acac)_3^+$ parent ion was $In(acac)_2^+$ in agreement with previous literature.[63] Subsequent time-dependent studies of In_2O_3 ALE utilized the $In(acac)_2^+$ ion signal.

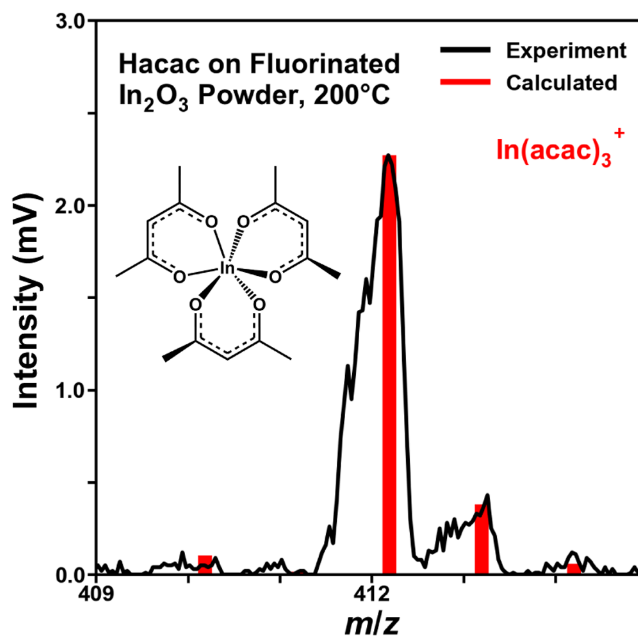

Figure 5. Mass spectrum of $In(acac)_3^+$ during Hacac exposure on fluorinated In_2O_3 at 200 °C. Experimental results are compared with a calculated mass spectrum assuming natural isotopic abundances.

Hacac exposures on fluorinated In_2O_3 could produce $In(acac)_3$ according to the chemical equation:

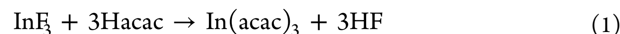

$$InF_3 + 3Hacac \rightarrow In(acac)_3 + 3HF \quad (1)$$

This reaction involves ligand substitution and hydrogen transfer. The ligand substitution is the exchange of fluorine on the indium metal center with an acac ligand to produce $In(acac)_3$. The hydrogen transfer is the transport of hydrogen from Hacac to fluorine to release HF. $In(acac)_3$ has been previously studied as a precursor for the atomic layer deposition (ALD) of indium oxy-sulfide films.[64,65] The thermal decomposition of $In(acac)_3$ can also be employed for the growth of indium−tin-oxide (ITO) films.[66]

The $In(acac)_3^+$ ion intensities in Figure 5 are in agreement with calculations based on the natural abundances of the indium isotopes. Indium has two prominent isotopes, ^{113}In at 4.3% and ^{115}In at 95.7%.[63] The largest signal at m/z 412 is attributed to $^{115}In(acac)_3$. The small signal present at m/z 410 is attributed to $^{113}In(acac)_3$. Carbon has two main isotopes, ^{12}C at 98.9% and ^{13}C at 1.1%. The small signals present at m/z 413 and 414 are attributed to the natural abundance of ^{13}C found in acac.

Figure 6 shows the time-resolved QMS results for $In(acac)_2^+$, H_2O^+, HF^+ and $Hacac^+$ obtained from several etch cycles using HF and Hacac exposures on In_2O_3 powder. Three consecutive exposures of Hacac were initially performed to remove any InF_3 present due to residual chamber fluorination. These three Hacac exposures also demonstrated that there was no spontaneous etching of In_2O_3 by Hacac. Three alternating cycles of HF and Hacac exposures were then performed after the three consecutive Hacac exposures.

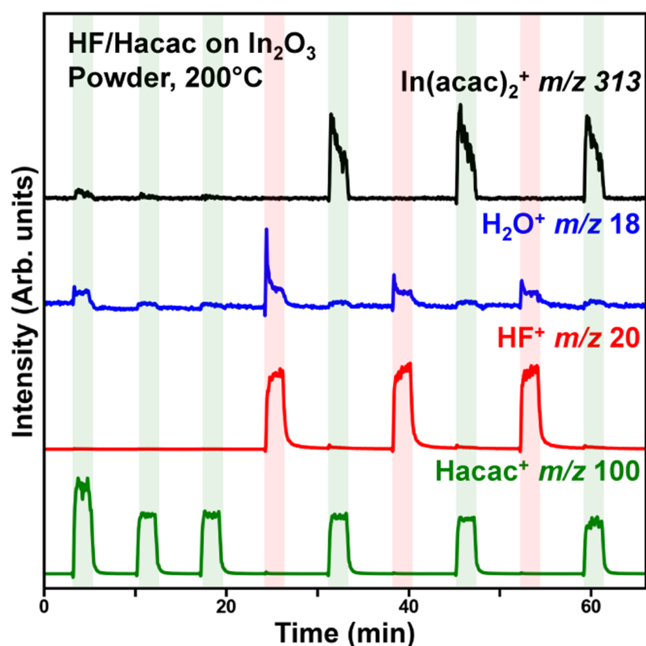

Figure 6. Time-resolved QMS results showing ion intensities for $In(acac)_2^+$, H_2O^+, HF^+, and $Hacac^+$ during Hacac and HF exposures on In_2O_3 at 200 °C. Shaded areas show duration of reactant exposures.

Figure 6 reveals that a H_2O^+ ion signal intensity coincides with the HF^+ ion intensity during the HF exposures. Figure 7a shows the relationship between the HF^+ and H_2O^+ ion signal intensities during the HF exposure. These results are consistent with the HF fluorination reaction:

$$In_2O_3 + 6HF \rightarrow 2InF_3 + 3\,H_2O \quad (2)$$

This reaction is expected because fluorination of In_2O_3 by HF is thermochemically favorable with $\Delta G°(200\ °C) = -373.7$ kJ.[67] The appearance of H_2O^+ ion signal prior to the HF^+ ion signal at the onset of the HF dose suggests that HF is consumed to produce H_2O as expected from the fluorination reaction.

The dominant ion signal intensity from each Hacac exposure after the HF exposures is $In(acac)_2^+$. This $In(acac)_2^+$ ion signal is the primary crack of the parent species, $In(acac)_3^+$.[63] There is also a small HF^+ ion signal intensity that coincides with the rising edge of the Hacac exposures in Figure 6. Figure 7b displays this correlation between the HF^+ and $Hacac^+$ ion signal intensities during the Hacac exposure. These results for the $In(acac)_2^+$ and HF^+ ion signals coinciding with the Hacac exposures are consistent with the ligand substitution and hydrogen transfer reaction given by eq 1

The appearance of HF as a volatile etch product during the Hacac exposure is surprising because HF is also the reactant

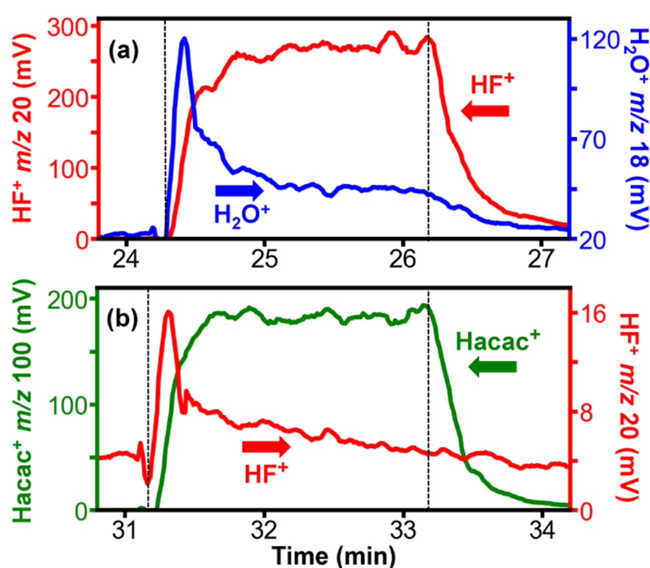

Figure 7. Ion intensities of a) H_2O^+ and HF^+ during a 120 s HF exposure on In_2O_3 at 200 °C and b) $Hacac^+$ and HF^+ during a 120 s Hacac exposure on fluorinated In_2O_3 at 200 °C. Vertical dashed lines indicate beginning and end of reactant exposures.

for fluorination of In_2O_3.[58] Some of the HF etch product could return and refluorinate the underlying In_2O_3 substrate.[58] This refluorination would reduce the amount of HF required to fluorinate the In_2O_3 surface. In the limit that all the HF etch product refluorinates the In_2O_3 substrate, the etching of fluorinated In_2O_3 by Hacac could become spontaneous. In this limit, the Hacac reaction would not be self-limiting.

Figure 6 reveals that the $In(acac)_2^+$ ion signal progressively decreases versus time during the individual Hacac exposures. This behavior suggests that the Hacac reaction is self-limiting. Figure 8 shows a close comparison between the $In(acac)_2^+$ and $Hacac^+$ ion signal intensities during the Hacac exposure. The $In(acac)_2^+$ ion signal decreases while the $Hacac^+$ ion signal remains constant. This behavior suggests that the Hacac

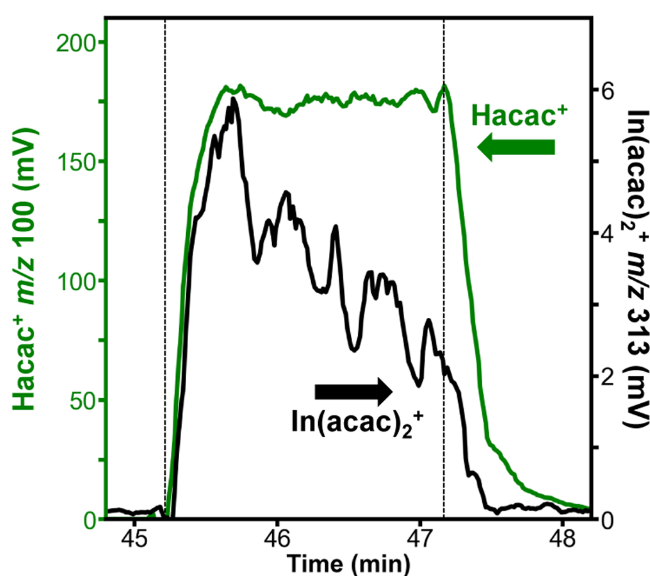

Figure 8. Ion intensities of $In(acac)_2^+$ and $Hacac^+$ during a 120 s Hacac exposure on In_2O_3 at 200 °C. Vertical dashed lines indicate beginning and end of Hacac exposure.

https://doi.org/10.1021/acs.jpcc.5c05730
J. Phys. Chem. C 2025, 129, 20223−20233

reaction is self-limiting even though the HF produced as an etch product could return to refluorinate the In_2O_3 surface.

3.3. Ga_2O_3 ALE Using HF and Hacac. Sequential exposures of HF and Hacac were also performed on Ga_2O_3 powder. Figure 9 shows the QMS results for experimental ion signal intensities at m/z 267 and 269 during Hacac exposure on fluorinated Ga_2O_3 powder. These ion signal intensities are consistent with $Ga(acac)_2^+$. The calculated ion intensities for $Ga(acac)_2^+$ are also displayed based on the natural abundances of the gallium isotopes. Gallium has two prominent isotopes, ^{69}Ga at 60.4% and ^{71}Ga at 39.6%.[63] The large peaks at m/z 267 and 269 in Figure 9 are assigned to $^{69}Ga(acac)_2^+$ and $^{71}Ga(acac)_2^+$, respectively. The small peaks at m/z 268 and 270 are attributed to the presence of ^{13}C in the acac ligands.

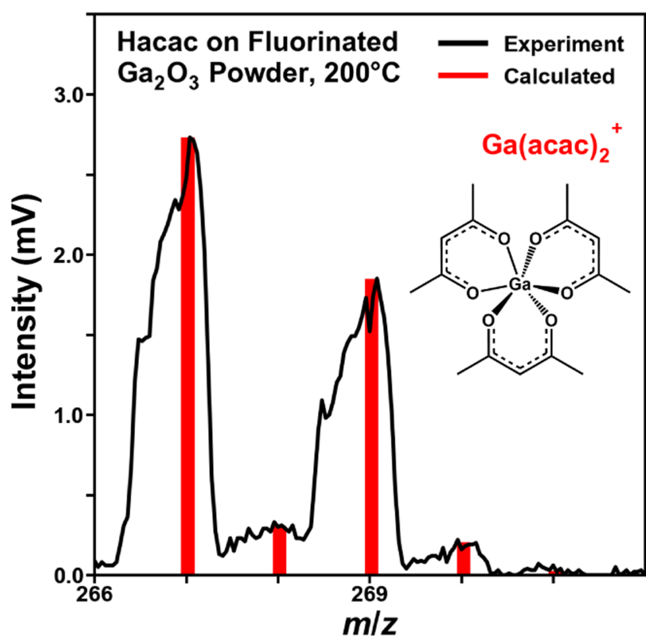

Figure 9. Mass spectrum of $Ga(acac)_2^+$ during Hacac exposure on fluorinated Ga_2O_3 at 200 °C. Experimental results are compared with a calculated mass spectrum assuming natural isotopic abundances.

$Ga(acac)_2^+$ is the largest cracking fragment of the $Ga(acac)_3^+$ parent ion.[63] The relative abundance of $Ga(acac)_2^+$ ion signal compared with the $Ga(acac)_3^+$ ion signal has been reported to be 81:2.[63] The agreement between the experimental and calculated spectra for $Ga(acac)_2^+$ in Figure 9 confirms the presence of $Ga(acac)_3$ as an etch product during Hacac exposures on the fluorinated Ga_2O_3 powder. $Ga(acac)_3$ is a well-known volatile Ga precursor. $Ga(acac)_3$ has been used as a precursor for Ga_2O_3 ALD.[68,69] $Ga(acac)_3$ is also a Ga source for Ga_2O_3 CVD.[70] Because the $Ga(acac)_2^+$ ion signal has a much larger intensity that $Ga(acac)_3^+$,[63] $Ga(acac)_2^+$ was used for the time-dependent QMS studies.

Figure 10 shows the time-resolved QMS results recorded during HF and Hacac exposures on Ga_2O_3 powder for the $Ga(acac)_2^+$, H_2O^+, HF^+, and $Hacac^+$ ion intensities. Initially, the Ga_2O_3 powder was subjected to three 2 min Hacac exposures. There was a 5 min purge between each Hacac exposure. The lack of any $Ga(acac)_2^+$ ion signal during these three Hacac exposures indicates that Hacac alone does not spontaneously etch Ga_2O_3.

Following the three Hacac exposures, the Ga_2O_3 powder was exposed to three sequential HF and Hacac exposures. A 2 min HF exposure was followed by a 2 min Hacac exposure. These exposures were separated by a 5 min purge. On the first HF exposure, Figure 10 reveals that the H_2O signal increases rapidly, suggesting fluorination of Ga_2O_3 according to

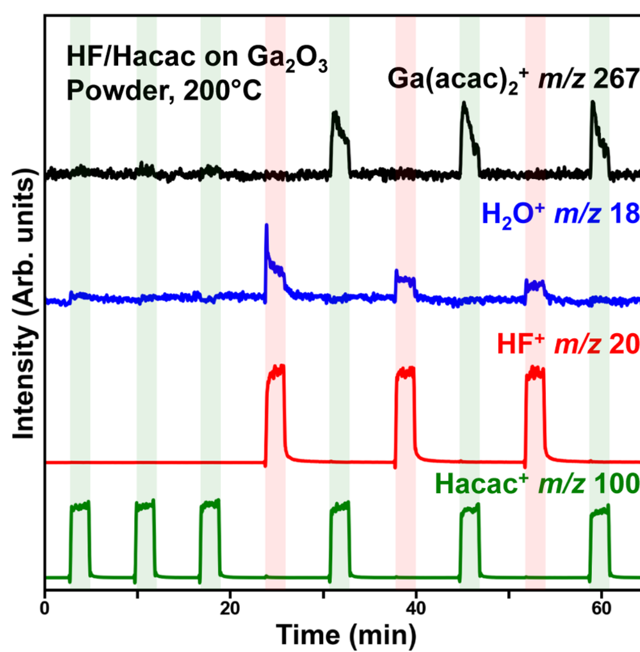

Figure 10. Time-resolved QMS results showing ion intensities of $Ga(acac)_2^+$, H_2O^+, HF^+, and $Hacac^+$ during Hacac and HF exposures on Ga_2O_3 at 200 °C. Shaded areas show duration of reactant exposures.

$$Ga_2O_3 + 6HF \rightarrow 2GaF_3 + 3H_2O \quad (3)$$

This reaction was anticipated because fluorination of Ga_2O_3 by HF is thermochemically favorable. The Gibbs free energy change for eq 3 is $\Delta G°(200\ °C) = -170.4$ kJ.[67] Figure 11a shows the relationship between the HF^+ and H_2O^+ ion signal intensities during the HF exposure. The H_2O^+ ion signal peaks on the rising edge of the HF^+ ion signal.

Figure 10 also shows that Hacac exposure on the fluorinated Ga_2O_3 powder produces a $Ga(acac)_2^+$ ion signal. The $Ga(acac)_2^+$ ion signal is consistent with $Ga(acac)_3$ as the primary etch product. Like the $In(acac)_3$ etch product observed during In_2O_3 ALE, the $Ga(acac)_3$ etch product is generated by the ligand substitution and hydrogen transfer reaction:

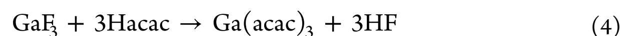

$$GaF_3 + 3Hacac \rightarrow Ga(acac)_3 + 3HF \quad (4)$$

The decrease in the $Ga(acac)_2^+$ signal versus time during the Hacac exposure is also consistent with a self-limiting reaction.

The Hacac exposure on the fluorinated Ga_2O_3 surface also produced HF as expected from eq 4. Figure 11b shows the relationship between the HF etch product and Hacac during the Hacac exposure. The HF^+ ion signal peaks on the rising edge of the $Hacac^+$ ion signal. Like the results in Figure 7b, HF is a volatile etch product from the reaction of Hacac with the fluorinated Ga_2O_3 surface. Some of the HF etch product could be retained and refluorinate the underlying Ga_2O_3 substrate. If all the HF etch product returned to refluorinate the Ga_2O_3 substrate, the etching of fluorinated Ga_2O_3 by Hacac could become spontaneous.

https://doi.org/10.1021/acs.jpcc.5c05730
J. Phys. Chem. C 2025, 129, 20223−20233

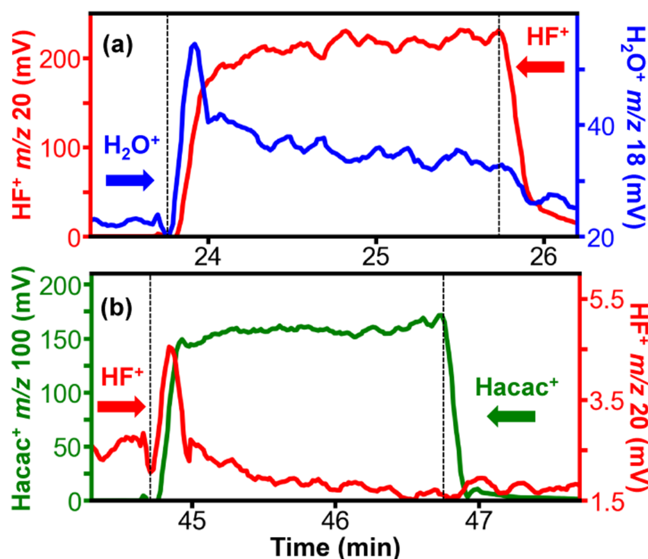

Figure 11. Ion intensities of a) H_2O^+ and HF^+ during a 120 s HF exposure on Ga_2O_3 at 200 °C and b) $Hacac^+$ and HF^+ during a 120 s Hacac exposure on fluorinated Ga_2O_3 at 200 °C. Vertical dashed lines indicate beginning and end of reactant exposures.

Figure 12 provides a closer look at the correlation between the $Hacac^+$ and $Ga(acac)_2{}^+$ ion intensities during one Hacac exposure. The $Hacac^+$ ion signal maintains a steady intensity throughout the entire 2 min Hacac exposure. In contrast, the $Ga(acac)_2{}^+$ ion signal decreases progressively during the Hacac exposure. This behavior is consistent with a self-limiting Hacac reaction during Hacac exposure on the fluorinated Ga_2O_3 surface.

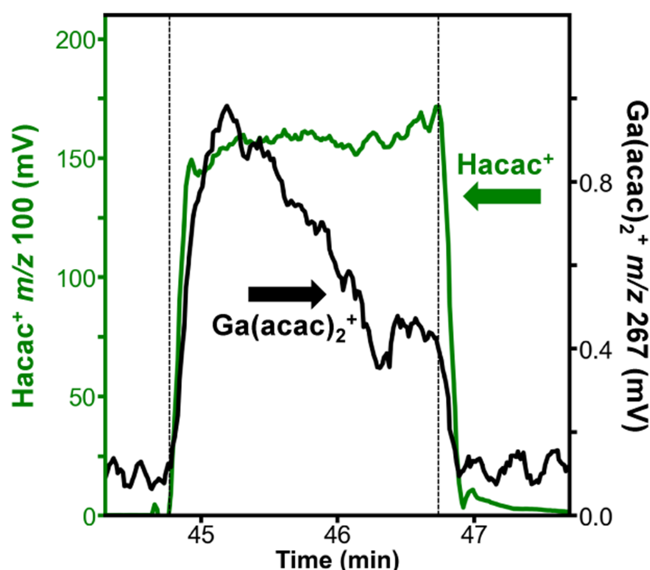

Figure 12. Ion intensities of $Ga(acac)_2{}^+$ and $Hacac^+$ during a 120 s Hacac exposure on Ga_2O_3 at 200 °C. Vertical dashed lines indicate beginning and end of Hacac exposure.

3.4. ZnO ALE Using HF and Hacac. To complete the study of all the constituent metal oxides in IGZO, exposures of HF and Hacac were also conducted on ZnO powder. Figure 13 shows the QMS results for the prominent experimental ion signal intensities at m/z 262, 264, 265, and 266 during Hacac exposure on fluorinated ZnO powder. These ion signal intensities are consistent with the mass spectrum of $Zn(acac)_2{}^+$. Zinc has four main isotopes, ^{64}Zn at 49.2%, ^{66}Zn at 27.7%, ^{67}Zn at 4.0% and ^{68}Zn at 18.5%. Figure 13 displays the calculated ion signals for $Zn(acac)_2$ based on the natural abundance of the zinc isotopes. There is excellent agreement between the experimental and calculated ion signals.

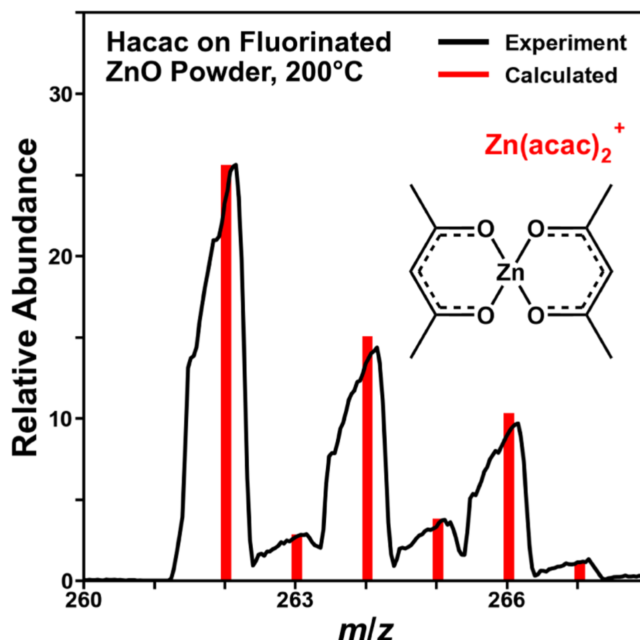

Figure 13. Mass spectrum of $Zn(acac)_2{}^+$ during Hacac exposure on fluorinated ZnO at 200 °C. Experimental results are compared with a calculated mass spectrum assuming natural isotopic abundances.

The ion signal intensities in Figure 13 at m/z 262, 264, 265, and 266 can be assigned to $^{64}Zn(acac)_2{}^+$, $^{66}Zn(acac)_2{}^+$, $^{67}Zn(acac)_2{}^+$ and $^{68}Zn(acac)_2{}^+$, respectively. The small peaks at m/z 263 and 267 result from ^{13}C naturally occurring in the acac ligands. The peak at m/z 265 is a combination of a small amount of naturally occurring ^{67}Zn, and ^{13}C existing in the acac ligands. The agreement of the calculated and experimental spectra confirmed that $Zn(acac)_2$ is the primary etch product of the reaction of Hacac with fluorinated ZnO. $Zn(acac)_2$ is a volatile precursor that has been employed for ZnO ALD and CVD.[71,72]

The ZnO powder was also subjected to sequential Hacac exposures to determine if Hacac can spontaneously etch ZnO. Figure 14 shows the results for three consecutive Hacac exposures on initial ZnO powder prior to HF fluorination. These 2 min Hacac exposures led to the immediate appearance of $Zn(acac)_2{}^+$ ion signals. The $Zn(acac)_2{}^+$ ion signal persists during each Hacac exposure. There is no indication of any reduction of the $Zn(acac)_2{}^+$ ion signal intensity versus Hacac exposure. These results are consistent with the previous observations that the Hacac reaction with ZnO is not self-limiting.[54,73] In contrast, earlier results claimed that the Hacac reaction with ZnO was self-limiting when performed sequentially with an O_2 plasma exposure.[55]

Following the three Hacac exposures, three cycles of alternating HF and Hacac exposures were performed on the ZnO powder. Each reactant exposure was conducted for 2 min and separated from the previous reactant exposure by a 5 min purge. For these alternating HF and Hacac exposures, Figure 14 shows that the fluorination of the ZnO powder by HF

https://doi.org/10.1021/acs.jpcc.5c05730
J. Phys. Chem. C 2025, 129, 20223−20233

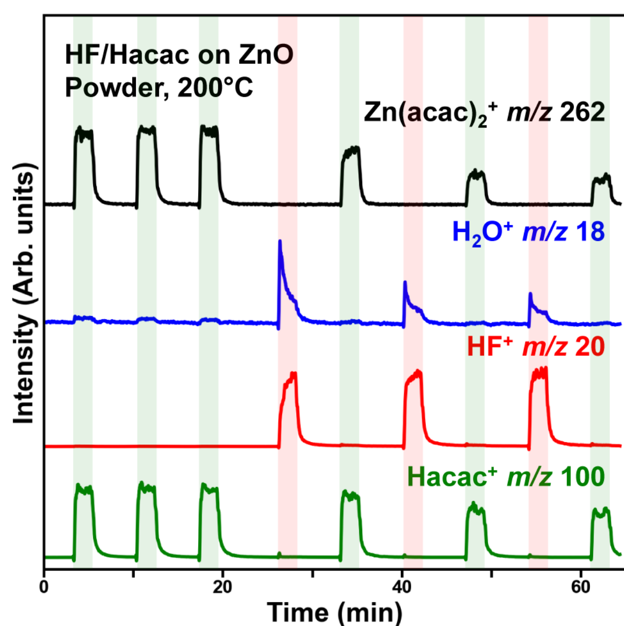

Figure 14. Time-resolved QMS data showing ion intensities of $Zn(acac)_2^+$, H_2O^+, HF^+, and $Hacac^+$ during Hacac and HF exposures on ZnO at 200 °C. Shaded areas show duration of reactant exposures.

decreased the intensity of the $Zn(acac)_2^+$ ion signal compared with the $Zn(acac)_2^+$ ion signals prior to fluorination. The fluorination of the ZnO to ZnF_2 produced less $Zn(acac)_2$ etch product compared with the $Zn(acac)_2$ etch product derived from the spontaneous etch of the ZnO powder.

The absence of self-limiting behavior during Hacac exposures is also illustrated by the comparison of the $Hacac^+$ and $Zn(acac)_2^+$ ion signals in Figure 15. During this Hacac exposure, the $Hacac^+$ and $Zn(acac)_2^+$ ion signals were fairly constant and tracked each other very closely. The time-dependent variations in the $Hacac^+$ ion signal also appeared in the $Zn(acac)_2^+$ ion signal. In contrast, the previous results for

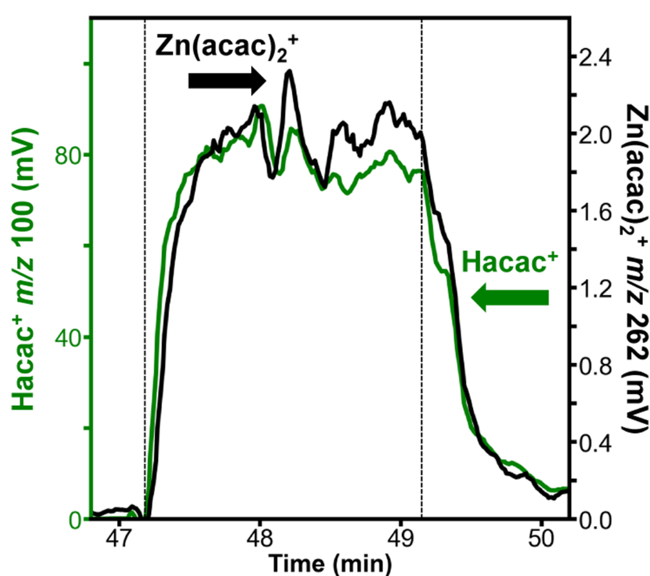

Figure 15. Ion intensities of $Zn(acac)_2^+$ and $Hacac^+$ during a 120 s Hacac exposure on ZnO at 200 °C. Vertical dashed lines indicate beginning and end of Hacac exposure.

the $Hacac^+$ and $In(acac)_2^+$ ion signals during In_2O_3 etching presented in Figure 8 and the $Hacac^+$ and $Ga(acac)_2^+$ ion signals during Ga_2O_3 etching displayed in Figure 12 both showed that the $In(acac)_2^+$ and $Ga(acac)_2^+$ ion signals decreased versus Hacac exposure. The lack of decrease for the $Zn(acac)_2^+$ ion signal in Figure 15 argues that Hacac is spontaneously etching ZnO.

The continuous etching observed for Hacac exposures on ZnO could influence the thermal ALE of IGZO using HF and Hacac exposures. However, Figure 3 shows that controlled etching of IGZO is observed using sequential HF and Hacac exposures. In addition, there was no etching of IGZO films using only Hacac exposures or alternating Hacac and O_3 exposures. The ability to etch IGZO in a self-limiting manner using sequential HF and Hacac exposures was not affected by the spontaneous etching of ZnO by Hacac exposures. The different environments for Zn in crystalline ZnO and amorphous IGZO may be responsible for these contrasting etching behaviors.

4. CONCLUSIONS

Sequential HF and Hacac exposures were employed to define the thermal ALE of IGZO, In_2O_3 and Ga_2O_3. In this thermal ALE process, HF first fluorinates the metal oxide surface to form a metal fluoride layer. Subsequently, the Hacac exposure reacts by ligand substitution and hydrogen transfer to volatilize the metal fluoride layer. The etching of IGZO films was demonstrated using *in situ* spectroscopic ellipsometry investigations. The volatile etch products during In_2O_3 and Ga_2O_3 thermal ALE were also identified using *in situ* quadrupole mass spectrometry studies.

The *in situ* spectroscopic ellipsometry investigations revealed that sequential exposures of HF and Hacac achieved IGZO etch rates of 0.3 Å/cycle at 200 °C. The IGZO etch rates were temperature dependent and increased to an etch rate of 0.6 Å/cycle at 250 °C. IGZO etching was also observed using Hhfac instead of Hacac. Sequential exposures of HF and Hhfac produced slightly lower etch rates of 0.2 Å/cycle at 230 °C. The etch rates were also temperature dependent and increased to an etch rate of 0.5 Å/cycle at 270 °C. In addition, control studies revealed that no etching occurred with repeated exposures of Hacac or sequential exposures of Hacac and O_3 on IGZO films up to 250 °C. Fluorination before the Hacac exposure was required for IGZO etching.

In situ quadrupole mass spectrometry (QMS) studies identified the volatile etch products produced during the etching of In_2O_3 and Ga_2O_3 powders by sequential HF and Hacac exposures at 200 °C. H_2O was monitored during HF fluorination of In_2O_3 and Ga_2O_3. $M(acac)_x$ species where M = In or Ga were detected as etch products during Hacac exposures on fluorinated In_2O_3 and Ga_2O_3. HF was also monitored during the Hacac exposures. These $M(acac)_x$ and HF etch products were consistent with a ligand substitution and hydrogen transfer mechanism.

The $In(acac)_3^+$ and $Ga(acac)_2^+$ ion signals were monitored during Hacac exposure on In_2O_3 and Ga_2O_3, respectively, during Hacac exposures after fluorination. The reduction of the $M(acac)_x^+$ ion signal intensity versus time during the Hacac exposure provided evidence for self-limiting surface reactions. In contrast to In_2O_3 and Ga_2O_3, Hacac exposures on ZnO led to spontaneous ZnO etching. The QMS studies revealed that constant $Zn(acac)_2^+$ ion signals were observed during Hacac exposure on ZnO powder. In spite of this spontaneous etching

of ZnO by Hacac, IGZO thermal ALE could still be achieved using sequential HF and Hacac exposures.

AUTHOR INFORMATION

Corresponding Author

Steven M. George − *Department of Chemistry, University of Colorado, Boulder, Colorado 80309, United States;* orcid.org/0000-0003-0253-9184; Email: Steven.George@Colorado.edu

Authors

Troy A. Colleran − *Department of Chemistry, University of Colorado, Boulder, Colorado 80309, United States*

Aziz I. Abdulagatov − *Department of Chemistry, University of Colorado, Boulder, Colorado 80309, United States*

Jonathan L. Partridge − *Department of Chemistry, University of Colorado, Boulder, Colorado 80309, United States;* orcid.org/0000-0002-0071-9854

Andrew S. Cavanagh − *Department of Chemistry, University of Colorado, Boulder, Colorado 80309, United States;* orcid.org/0000-0002-6201-530X

Complete contact information is available at: https://pubs.acs.org/10.1021/acs.jpcc.5c05730

Notes

The authors declare no competing financial interest.

ACKNOWLEDGMENTS

This work was supported by the Center for Heterogeneous Integration of Micro Electronic Systems (CHIMES), one of the seven centers sponsored by the Semiconductor Research Corporation (SRC) and DARPA under the Joint University Microelectronics Program 2.0 (JUMP 2.0). Lam Research also contributed funding for the QMS apparatus and the QMS investigations.

REFERENCES

(1) Nomura, K.; Ohta, H.; Takagi, A.; Kamiya, T.; Hirano, M.; Hosono, H. Room-Temperature Fabrication of Transparent Flexible Thin-Film Transistors Using Amorphous Oxide Semiconductors. *Nature* **2004**, *432*, 488−492.

(2) Zhu, Y.; He, Y. L.; Jiang, S. S.; Zhu, L.; Chen, C. S.; Wan, Q. Indium-Gallium-Zinc-Oxide Thin-Film Transistors: Materials, Devices, and Applications. *J. Semicond.* **2021**, *42*, 031101.

(3) Ajayan, J.; Sreejith, S.; Kumari, N. A.; Manikandan, M.; Sen, S.; Kumar, M. Amorphous Indium Gallium Zinc Oxide Thin Film Transistors (a-IGZO-TFTs): Exciting Prospects and Fabrication Challenges. *Microelectron. Eng.* **2025**, *298*, 112327.

(4) Woods-Robinson, R.; Han, Y. B.; Zhang, H. Y.; Ablekim, T.; Khan, I.; Persson, K. A.; Zakutayev, A. Wide Band Gap Chalcogenide Semiconductors. *Chem. Rev.* **2020**, *120*, 4007−4055.

(5) Jeong, J. K.; Jeong, J. H.; Yang, H. W.; Park, J.-S.; Mo, Y.-G.; Kim, H. D. High Performance Thin Film Transistors With Cosputtered Amorphous Indium Gallium Zinc Oxide Channel. *Appl. Phys. Lett.* **2007**, *91*, 113505.

(6) Nomura, K. Recent Progress of Oxide-TFT-Based Inverter Technology. *J. Inf. Dispersion* **2021**, *22*, 211−229.

(7) Eadi, S. B.; Shin, H. J.; Song, K. W.; Choi, H. W.; Lee, H. D. Sensing Properties of Indium-Gallium-Zinc-Oxide Thin Films under the Influence of Thickness and Annealing Ambient. *J. Electrochem. Soc.* **2021**, *168*, 067512.

(8) Petti, L.; Münzenrieder, N.; Vogt, C.; Faber, H.; Büthe, L.; Cantarella, G.; Bottacchi, F.; Anthopoulos, T. D.; Tröster, G. Metal Oxide Semiconductor Thin-Film Transistors for Flexible Electronics. *Appl. Phys. Rev.* **2016**, *3*, 021303.

(9) Han, K. Z.; Kong, Q. W.; Kang, Y. Y.; Sun, C.; Wang, C. K.; Zhang, J. S.; Xu, H. W.; Samanta, S.; Zhou, J. R.; Wang, H. B.; Thean, A. V. Y.; Gong, X. Indium-Gallium-Zinc-Oxide (IGZO) Nanowire Transistors. *IEEE Trans. Electron Devices* **2021**, *68*, 6610−6616.

(10) Park, J.-S.; Jeong, J. K.; Mo, Y.-G.; Kim, H. D.; Kim, C.-J. Control of Threshold Voltage in ZnO-Based Oxide Thin Film Transistors. *Appl. Phys. Lett.* **2008**, *93*, 033513.

(11) Sheng, J.; Hong, T.; Lee, H. M.; Kim, K.; Sasase, M.; Kim, J.; Hosono, H.; Park, J. S. Amorphous IGZO TFT with High Mobility of ~ 70 $cm^2/(V\ s)$ via Vertical Dimension Control Using PEALD. *ACS Appl. Mater. Interfaces* **2019**, *11*, 40300−40309.

(12) Wang, Y.; Sun, X. W.; Goh, G. K. L.; Demir, H. V.; Yu, H. Y. Influence of Channel Layer Thickness on the Electrical Performances of Inkjet-Printed In-Ga-Zn Oxide Thin-Film Transistors. *IEEE Trans. Electron Devices* **2011**, *58*, 480−485.

(13) Li, Y.; Pei, Y. L.; Hu, R.; Chen, Z. M.; Zhao, Y.; Shen, Z.; Fan, B. F.; Liang, J.; Wang, G. Effect of Channel Thickness on Electrical Performance of Amorphous IGZO Thin-Film Transistor With Atomic Layer Deposited Alumina Oxide Dielectric. *Curr. Appl. Phys.* **2014**, *14*, 941−945.

(14) Li, X. D.; Chen, S.; Chen, T. P.; Liu, Y. Thickness Dependence of Optical Properties of Amorphous Indium Gallium Zinc Oxide Thin Films: Effects of Free-Electrons and Quantum Confinement. *ECS Solid State Lett.* **2015**, *4* (3), P29.

(15) Shin, W.; Kwon, D.; Ryu, M.; Kwon, J.; Hong, S.; Jeong, Y.; Jung, G.; Park, J.; Kim, D.; Lee, J. H. Effects of IGZO Film Thickness on H_2S Gas Sensing Performance: Response, Excessive Recovery, Low-Frequency Noise, and Signal-To-Noise Ratio. *Sens. Actuators, B* **2021**, *344*, 130148.

(16) Cho, M. H.; Seol, H.; Yang, H.; Yun, P. S.; Bae, J. U.; Park, K. S.; Jeong, J. K. High-Performance Amorphous Indium Gallium Zinc Oxide Thin-Film Transistors Fabricated by Atomic Layer Deposition. *IEEE Electron Device Lett.* **2018**, *39*, 688−691.

(17) Sheng, J.; Lee, H. J.; Oh, S.; Park, J. S. Flexible and High-Performance Amorphous Indium Zinc Oxide Thin-Film Transistor Using Low-Temperature Atomic Layer Deposition. *ACS Appl. Mater. Interfaces* **2016**, *8*, 33821−33828.

(18) Sheng, J.; Lee, J.-H.; Choi, W.-H.; Hong, T.; Kim, M.; Park, J.-S. Review Article: Atomic Layer Deposition for Oxide Semiconductor Thin Film Transistors: Advances in Research and Development. *J. Vac. Sci. Technol., A* **2018**, *36*, 060801.

(19) Kim, J. K.; Kim, J. Y.; Han, S. C.; Kwak, J. S.; Kim, H. K.; Lee, J. M. Wet Chemical Etching of Zn-Containing Oxide and HfO_2 Films. *J. Electrochem. Soc.* **2010**, *157*, D462−D465.

(20) Lee, C. Y.; Chang, C.; Shih, W. P.; Dai, C. L. Wet Etching Rates Of InGaZnO for the Fabrication of Transparent Thin-Film Transistors on Plastic Substrates. *Thin Solid Films* **2010**, *518*, 3992−3998.

(21) Chini, S. F.; Amirfazli, A. Understanding Pattern Collapse in Photolithography Process Due to Capillary Forces. *Langmuir* **2010**, *26*, 13707−13714.

(22) Joo, Y. H.; Woo, J. C.; Kim, C. I. A Study of the Surface Chemical Reactions on IGZO Thin Film in BCl_3/Ar Inductively Coupled Plasma. *J. Electrochem. Soc.* **2012**, *159*, D190−D195.

(23) Park, J. C.; Jeong, O. G.; Kim, J. K.; Yun, Y. H.; Pearton, S. J.; Cho, H. Comparison of Chlorine- and Fluorine-Based Inductively Coupled Plasmas for Dry Etching of $InGaZnO_4$ Films. *Thin Solid Films* **2013**, *546*, 136−140.

(24) Park, W.; Whang, K.-W.; Yoon, Y. G.; Kim, J. H.; Rha, S. H.; Hwang, C. S. High Rate Dry Etching of InGaZnO By BCl_3/O_2 Plasma. *Appl. Phys. Lett.* **2011**, *99*, 062110.

(25) Kim, K.; Efremov, A.; Lee, J.; Kwon, K- H.; Yeom, G. Y. Etching Mechanisms of (In, Ga, Zn)O Thin Films in $CF_4/Ar/O_2$ Inductively Coupled Plasma. *J. Vac. Sci. Technol., A* **2015**, *33*, 031601.

(26) Edel, R.; Alexander, E.; Nam, T.; Cavanagh, A. S.; Van Voorhis, T.; George, S. M. Removing Defects from Sputter damage on InGaP Surfaces Using Thermal Atomic Layer Etching. *J. Vac. Sci. Technol., A* **2024**, *42*, 062602.

(27) Pang, S. W. Surface Damage on GaAs Induced by Reactive Ion Etching and Sputter Etching. *J. Electrochem. Soc.* **1986**, *133*, 784−787.
(28) Shul, R. J.; Zhang, L.; Baca, A. G.; Willison, C. G.; Han, J.; Pearton, S. J.; Ren, F. Inductively Coupled Plasma-Induced Etch Damage of GaN p-n Junctions. *J. Vac. Sci. Technol., A* **2000**, *18*, 1139−1143.
(29) Fischer, A.; Routzahn, A.; George, S. M.; Lill, T. Thermal Atomic Layer Etching: A Review. *J. Vac. Sci. Technol., A* **2021**, *39*, 030801.
(30) Kanarik, K. J.; Lill, T.; Hudson, E. A.; Sriraman, S.; Tan, S.; Marks, J.; Vahedi, V.; Gottscho, R. A. Overview of Atomic Layer Etching in the Semiconductor Industry. *J. Vac. Sci. Technol., A* **2015**, *33*, 020802.
(31) George, S. M. Mechanisms of Thermal Atomic Layer Etching. *Acc. Chem. Res.* **2020**, *53*, 1151−1160.
(32) George, S. M.; Lee, Y. Prospects for Thermal Atomic Layer Etching Using Sequential, Self-Limiting Fluorination and Ligand-Exchange Reactions. *ACS Nano* **2016**, *10*, 4889−4894.
(33) Lee, Y.; DuMont, J. W.; George, S. M. Trimethylaluminum as the Metal Precursor for the Atomic Layer Etching of Al_2O_3 Using Sequential, Self-Limiting Thermal Reactions. *Chem. Mater.* **2016**, *28*, 2994−3003.
(34) Lee, Y.; George, S. M. Atomic Layer Etching of Al_2O_3 Using Sequential, Self-Limiting Thermal Reactions with $Sn(acac)_2$ and Hydrogen Fluoride. *ACS Nano* **2015**, *9*, 2061−2070.
(35) Murdzek, J. A.; Rajashekhar, A.; Makala, R. S.; George, S. M. Thermal Atomic Layer Etching of Amorphous and Crystalline Al_2O_3 Films. *J. Vac. Sci. Technol., A* **2021**, *39*, 042602.
(36) Lee, Y.; DuMont, J. W.; George, S. M. Mechanism of Thermal Al_2O_3 Atomic Layer Etching Using Sequential Reactions with $Sn(acac)_2$ and HF. *Chem. Mater.* **2015**, *27*, 3648−3657.
(37) Lee, Y.; DuMont, J. W.; George, S. M. Atomic Layer Etching of AlF_3 Using Sequential, Self-Limiting Thermal Reactions with $Sn(acac)_2$ and Hydrogen Fluoride. *J. Phys. Chem. C* **2015**, *119*, 25385−25393.
(38) Lee, Y.; DuMont, J. W.; George, S. M. Atomic Layer Etching of HfO_2 Using Sequential, Self-Limiting Thermal Reactions with $Sn(acac)_2$ and HF. *ECS J. Solid State Sci. Technol.* **2015**, *4*, N5013−N5022.
(39) Lee, Y.; George, S. M. Thermal Atomic Layer Etching of HfO_2 Using HF for Fluorination And TCl_4 for Ligand-Exchange. *J. Vac. Sci. Technol., A* **2018**, *36* (6), 061504.
(40) Lee, Y.; George, S. M. Thermal Atomic Layer Etching of Al_2O_3, HfO_2, and ZrO_2 Using Sequential Hydrogen Fluoride and Dimethylaluminum Chloride Exposures. *J. Phys. Chem. C* **2019**, *123*, 18455−18466.
(41) Murdzek, J. A.; Lii-Rosales, A.; George, S. M. Thermal Atomic Layer Etching of Nickel Using Sequential Chlorination and Ligand-Addition Reactions. *Chem. Mater.* **2021**, *33*, 9174−9183.
(42) Murdzek, J. A.; Lii-Rosales, A.; George, S. M. Thermal Atomic Layer Etching of Cobalt Using Sulfuryl Chloride for Chlorination and Tetramethylethylenediamine or Trimethylphosphine for Ligand Addition. *J. Vac. Sci. Technol., A* **2023**, *41*, 032603.
(43) Partridge, J. L.; Murdzek, J. A.; Johnson, V. L.; Cavanagh, A. S.; Fischer, A.; Lill, T.; Sharma, S.; George, S. M. Thermal Atomic Layer Etching of CoO, ZnO, Fe_2O_3, and NiO by Chlorination and Ligand Addition Using SO_2Cl_2 and Tetramethylethylenediamine. *Chem. Mater.* **2023**, *35*, 2058−2068.
(44) Johnson, N. R.; George, S. M. WO_3 and W Thermal Atomic Layer Etching Using "Conversion-Fluorination" and "Oxidation-Conversion-Fluorination" Mechanisms. *ACS Appl. Mater. Interfaces* **2017**, *9*, 34435−34447.
(45) Cano, A. M.; Natarajan, S. K.; Partridge, J. L.; Elliott, S. D.; George, S. M. Spontaneous Etching of B_2O_3 By HF Gas Studied Using Infrared Spectroscopy, Mass Spectrometry, and Density Functional Theory. *J. Vac. Sci. Technol., A* **2022**, *40*, 022601.
(46) Cano, A. M.; Partridge, J. L.; George, S. M. Thermal Atomic Layer Etching of Al_2O_3 Using Sequential HF and BCl_3 Exposures: Evidence for Combined Ligand-Exchange and Conversion Mechanisms. *Chem. Mater.* **2022**, *34*, 6440−6449.
(47) Abdulagatov, A. I.; George, S. M. Thermal Atomic Layer Etching of Silicon Using O_2, HF, and $Al(CH_3)_3$ as the Reactants. *Chem. Mater.* **2018**, *30*, 8465−8475.
(48) Abdulagatov, A. I.; George, S. M. Thermal Atomic Layer Etching of Silicon Nitride Using an Oxidation and "Conversion Etch" Mechanism. *J. Vac. Sci. Technol., A* **2020**, *38*, 022607.
(49) Abdulagatov, A. I.; Sharma, V.; Murdzek, J. A.; Cavanagh, A. S.; George, S. M. Thermal Atomic Layer Etching of Germanium-Rich SiGe Using an Oxidation and "Conversion-Etch" Mechanism. *J. Vac. Sci. Technol., A* **2021**, *39*, 022602.
(50) DuMont, J. W.; Marquardt, A. E.; Cano, A. M.; George, S. M. Thermal Atomic Layer Etching of SiO_2 by a "Conversion-Etch" Mechanism Using Sequential Reactions of Trimethylaluminum and Hydrogen Fluoride. *ACS Appl. Mater. Interfaces* **2017**, *9*, 10296−10307.
(51) Droes, S. R.; Kodas, T. T.; Hampden-Smith, M. J. Dry Etching of ZnO Films with Hexafluoroacetylacetone. *Adv. Mater.* **1998**, *10*, 1129−1133.
(52) Farkas, J.; Chi, K. M.; Hampden-Smith, M. J.; Kodas, T. T.; Dubois, L. H. Etching of Copper and Copper-Oxide at High-Rates via Generation of Volatile Copper Species. *Mater. Sci. Eng., B* **1993**, *17*, 93−96.
(53) George, M. A.; Hess, D. W.; Beck, S. E.; Young, K.; Bohling, D. A.; Voloshin, G.; Lane, A. P. Reaction of 1,1,1,5,5,5-Hexafluoro-2,4-Pentanedione (Hhfac) with Iron and Iron Oxide Thin Films. *J. Electrochem. Soc.* **1996**, *143* (143), 3257−3266.
(54) Partridge, J. L.; Abdulagatov, A. I.; Zywotko, D. R.; George, S. M. Limiting or Continuous Thermal Etching of First Row Transition Metal Oxides Using Acetylacetone and Ozone. *Chem. Mater.* **2024**, *36*, 7151−7161.
(55) Mameli, A.; Verheijen, M. A.; Mackus, A. J. M.; Kessels, W. M. M.; Roozeboom, F. Isotropic Atomic Layer Etching of ZnO Using Acetylacetone and O_2 Plasma. *ACS Appl. Mater. Interfaces* **2018**, *10*, 38588−38595.
(56) Partridge, J. L.; Abdulagatov, A. I.; Sharma, V.; Murdzek, J. A.; Cavanagh, A.; George, S. M. Thermal Atomic Layer Etching of CoO Using Acetylacetone and Ozone: Evidence for Changes in Oxidation State and Crystal Structure during Sequential Exposures. *Appl. Surf. Sci.* **2023**, *638*, 157923.
(57) Chen, J. K.-C.; Altieri, N. D.; Kim, T.; Chen, E.; Lill, T.; Shen, M.; Chang, J. P. Directional Etch of Magnetic and Noble Metals. II. Organic Chemical Vapor Etch. *J. Vac. Sci. Technol., A* **2017**, *35* (5), 05C305.
(58) Colleran, T. A.; Abdulagatov, A. I.; Partridge, J. L.; Cavanagh, A. S.; George, S. M. Mechanism of Thermal Atomic Layer Etching of Hafnium Zirconium Oxide, HfO_2 and ZrO_2 Using Sequential HF and Acetylacetone Exposures. *Chem. Mater.* **2025**, *37*, 5935−5945.
(59) Kim, Y.; Chae, S.; Ha, H.; Lee, H.; Lee, S.; Chae, H. Thermal Atomic Layer Etching of Cobalt Using Plasma Chlorination and Chelation with Hexafluoroacetylacetone. *Appl. Surf. Sci.* **2023**, *619*, 156751.
(60) Konh, M.; He, C.; Lin, X.; Guo, X.; Pallem, V.; Opila, R. L.; Teplyakov, A. V.; Wang, Z.; Yuan, B. Molecular Mechanisms of Atomic Layer Etching of Cobalt with Sequential Exposure to Molecular Chlorine and Diketones. *J. Vac. Sci. Technol., A* **2019**, *37*, 021004.
(61) Lii-Rosales, A.; Cavanagh, A. S.; Fischer, A.; Lill, T.; George, S. M. Spontaneous Etching of Metal Fluorides Using Ligand-Exchange Reactions: Landscape Revealed by Mass Spectrometry. *Chem. Mater.* **2021**, *33*, 7719−7730.
(62) Kung, H.; Teplyakov, A. Selectivity and Mechanism of Thermal Decomposition of beta-Diketones on ZnO Powder. *J. Catal.* **2015**, *330*, 145−153.
(63) Charalambous, J.; Gossett, R. G.; Johri, M. H.; Kensett, M. J. Mass-Spectra of Tris(Beta-Diketonato)Gallium(III) And Tris(Beta-Diketonato)Indium(III). *Inorg. Chim. Acta* **1977**, *22*, 101−105.

(64) Bugot, C.; Schneider, N.; Bouttemy, M.; Etcheberry, A.; Lincot, D.; Donsanti, F. Study of Atomic Layer Deposition of Indium Oxy-Sulfide Films for Cu(In,Ga)Se_2 Solar Cells. *Thin Solid Films* **2015**, *582*, 340−344.
(65) Bugot, C.; Schneider, N.; Lincot, D.; Donsanti, F. Synthesis of Indium Oxi-Sulfide Films by Atomic Layer Deposition: The Essential Role of Plasma Enhancement. *Beilstein J. Nanotechnol.* **2013**, *4*, 750−757.
(66) Nomura, R.; Inazawa, S.; Matsuda, H.; Saeki, S. Thermal-Decomposition of Organoindium Compounds and Preparation of Indium Tin-Oxide Films. *Polyhedron* **1987**, *6*, 507−512.
(67) Roine, A. *HSC Chemistry 9.9.2.3*; Outokumpu Research Oy: Pori, Finland, 2019.
(68) Dezelah, C. L.; Niinistö, J.; Arstila, K.; Niinistö, L.; Winter, C. H. Atomic Layer Deposition of Ga_2O_3 Films from a Dialkylamido-Based Precursor. *Chem. Mater.* **2006**, *18* (2), 471−475.
(69) Nieminen, M.; Niinistö, L.; Rauhala, E. Growth of Gallium Oxide Thin Films From Gallium Acetylacetonate by Atomic Layer Epitaxy. *J. Mater. Chem.* **1996**, *6*, 27−31.
(70) Yasuoka, T.; Liu, L.; Dang, G. T.; Kawaharamura, T. Growth of α-Ga_2O_3 from Gallium Acetylacetonate under HCl Support by Mist Chemical Vapor Deposition. *Nanomaterials* **2024**, *14*, 1221.
(71) Yim, J.; Haimi, E.; Mäntymäki, M.; Kärkäs, V.; Bes, R.; Gutierrez, A. A.; Meinander, K.; Brüner, P.; Grehl, T.; Gell, L.; et al. Atomic Layer Deposition of Zinc Oxide on Mesoporous Zirconia Using Zinc(II) Acetylacetonate and Air. *Chem. Mater.* **2023**, *35* (19), 7915−7930.
(72) Sato, H.; Minami, T.; Miyata, T.; Takata, S.; Ishii, M. Transparent Conducting ZnO Thin-Films Prepared on Low-Temperature Substrates by Chemical Vapor Deposition Using $Zn(C_5H_7O_2)_2$. *Thin Solid Films* **1994**, *246*, 65−70.
(73) McNealy-James, T.; Mangroo, R.; Berriel, S. N.; Tomar, L.; Bissell, E.; Currie, T. M.; Moore, J.; Jurca, T.; Banerjee, P. In situ, Simultaneous Spectroscopic Ellipsometry and Quadrupole Mass Spectrometry Studies of ZnO Etching Using Hacac and O_2 Plasma. *J. Vac. Sci. Technol., A* **2025**, *43*, 042602.

CAS BIOFINDER DISCOVERY PLATFORM™
BRIDGE BIOLOGY AND CHEMISTRY FOR FASTER ANSWERS
Analyze target relationships, compound effects, and disease pathways
Explore the platform

https://doi.org/10.1021/acs.jpcc.5c05730
J. Phys. Chem. C 2025, 129, 20223−20233